〔Articles〕

Heat Transfer Characteristics of Mini-sized Throttle Elements in Gaseous Cooling; Minichannel, Mini-orifice and Mini-slit

Kazuo HARA*

Abstract

The heat transfer characteristics of three kinds of mini sized elements were investigated. These were minichannel, mini-orifice and mini-slit. Rectangular mini-orifices were machined along the periphery of a circular aluminum disk, which was set inside the thick cylinder made oxygen free copper to of compose the mini-orifice. Mini-slit was constructed between the cylinder and circular disks of smaller diameter than the cylinder inner diameter. Electric heaters heated the cylinder. Mini-slit and mini-orifice disks were replaced to vary flow parameters extensively. Minichannel array was machined in the oxygen free copper block. Two blocks were stacked to compose on impingement heat transfer system. System pressure was modified for 1 and 4 atmosphere in all experiments.

The exit temperature decreased as the mass flow rate increased for all the test configurations. In other words, dimensionless temperature decreased linearly with logarithm of Reynolds number and almost unchanged for system pressure of 1 and 4 atmosphere. The dimensionless temperature increased as the hydraulic diameter of the elements became small and as the distance between elements increased.

The dimensionless temperature of impingement cooling was also not affected by the system pressure variation, although the momentum of the jet decreased with increasing system pressure. This suggests that the fundamental character of the impingement heat transfer was a stagnation flow heat transfer.

INTRODUCTION

The reader may refer to the introduction of Hara et al (2006) about the background, the experimental works and the numerical calculations because of duplication.

The author[1] showed that high heat transfer coefficient could be achieved in the minichannel diameter of about 1 mm. The performance of turbulent channel flow heat transfer, however, may not greatly differ from Dittus-Boelter correlation. There may be a certain heat transfer mechanism if the coefficient exceeds that of the correlation. Author[2] showed that the reason was the thermal convection around the inlet region of the channel.

Orifices of small sizes are widely used in the gas turbine cooling elements. Air flow is throttled at relatively high pressure ratio. This paper focuses on the heat transfer of small size orifice or channel and describes the heat transfer dependency on the size of the elements, namely, mini sized orifice and slit. The heat transfer performance of the inlet part of the minichannel was estimated by applying certain assumption and was compared with orifices and slits, because the heat transfer of the minichannel is considered to be the sum of the thermal convection from channel inlet region and inside of the channel.

The convective heat transfer is classified as a kind of thermal conduction. The heat transfer performance is determined by Fourier's law of heat transfer on the solid boundary, if the lami-

*交通機械工学科
平成20年6月30日受理

nar sub-layer covers the solid surface. This suggests that heat transfer depends on the contact between solid surface and large part of passing air as possible. In the minichannel inlet region, more air can contact with solid surface than channel of ordinary size, because the ratio of wetted perimeter length to cross-sectional area is large.

It is difficult to get the local temperature or heat flux distribution, because of the small size. Only the temperature of inlet and outlet can generally be measured, and therefore it is difficult to get direct evidence to explain the experimental result. The dimensions of the elements, pressure ratios and system pressures were varied widely in this work to get characteristics of mini sized heat transfer elements.

The pumping power of coolant should be minimized in the cooling system. The ratio of convected energy to pumping power is called *COP* (coefficient of power) and one of the important index of heat exchanger system. In this paper, however, large value of heat transfer performance is emphasized rather than energy consumption or pressure drop of the element. The heat transfer of the mini sized elements have been investigated, since the heat transfer mechanism is expected to be similar to the minichannel.

Orifice plate is not generally considered as a heat transfer element, because conductive heat supply is not expected through the metal. But there is a possibility of high local heat flux if a small orifice is set vertically and flush with the heated surface. The author call this mini-orifice.

Similar phenomena can be expected when air is flowed through mini sized slit. The ratio of wetted perimeter length to cross-sectional area of the gap also becomes large. This is called mini-slit in this paper. Mini-orifice was investigated from the point of view of the practical use, while the mini-slit was investigated for clarifying the heat transfer dependency on its dimension.

NOMENCLATURE

Symbol	Description	Unit
A	area of a channel or a passage	m^2
	coefficient of linear regression	-
B	coefficient of linear regression	-
a	width of orifice, see Figure 2	m
b	depth of orifice, see Figure 2	m
c	clearance = $(d\text{-}D)/2$, see Table 2	m
COP	coefficient of power	-
C_p	specific heat of air	J/kgK
D	diameter of minichannel or disk	m
d	inner diameter of the cylinder =29mm	m
D_h	hydraulic diameter of element	m
dx	distance of mini-orifice disks =2.3mm	m
H	impingement distance =2.5mm	-
h	mean heat transfer coefficient	J/m^2K
i, j, k	subscript of orthogonal coordinate	-
L	length of the channel	m
m	mass flow rate for a single element	kg/s
N	number of minichannel or elements in a disk	-
N_u	Nusselt number	-
P_1	total pressure of the upstream plenum	Pa
P_2	total pressure of the downstream plenum	Pa
R_e	Reynolds number	-
S	spacing between two elements	m
S_t	channel Stanton number	-
S_{t1}	local Stanton number on wall 3	-
T_1	total temperature of the upstream plenum	K
T_2	total temperature of the downstream plenum	K
T_w	wall temperature	K
u	mean velocity of the minichannel	m/s
	velocity in Equation (9) and (10)	m
W	heat flux across a wall 3	W/m^2
W_k	Truesdell kinematic vorticity number	-
x	distance from cylinder edge, Figure 1	m
	orthogonal coordinate in Equation (9) and (10)	m
κ	specific heat ratio	-
μ	viscosity of air	Pa s
ρ	density of air	kg/m^3
θ	dimensionless temperature	-
θ_c	dimensionless temperature due to inside of channel	-
θ_1	dimensionless temperature due to channel inlet	-

EXPERIMENTAL APPARATUS AND METHOD

The author used three kinds of heat transfer elements for the experiment, which were mini-channel, mini-orifice and mini-slit. Figure 1 is a sectional view for both mini-orifice and mini-slit test equipment with oxygen free copper cylinder of 60 mm outer diameter, 29 mm inner diameter and 26 mm height, which were heated by electric heaters, and heat was convected to the passing air. An aluminum disk of 1 mm thick was installed in the cylinder to form a flow field of mini-slit and mini-orifice between the cylinder and the disk. The disk was supported by a support plate with semicircular perforation and a screw of 3 mm diameter at a distance of $x=11$ mm from the edge of the cylinder. The aluminum disk was cut by means of a CO_2 laser beam machine and had high accuracy of diameter.

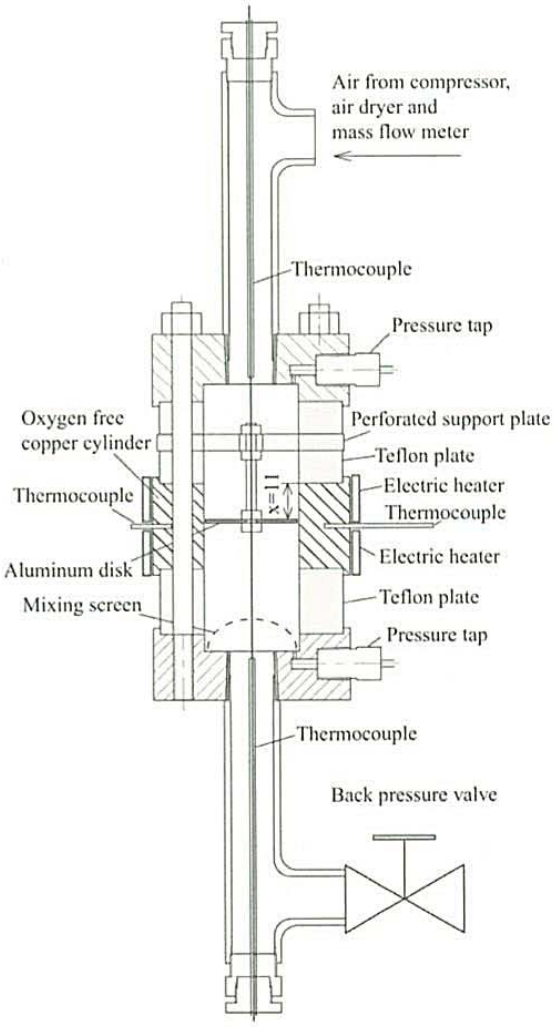

Figure 1 Cross section of mini-orifice and mini-slit equipment

Figure 2 shows the configuration of mini-orifice, which was sawed by metal saw of 1 mm thickness. Table 1 lists a number of orifices N, width a and depth b. The spacing S is defined as $S=\pi d/N$. The dimensional accuracy of the orifices were not so good, because the author worked them. But the variation of the dimensions were so large that dimensional variations exceeded the accuracy of manufacturing. There must be a minute clearance between cylinder and circular part of the disk to set it in the cylinder, but the flow rate through the minute clearance was impossible to measure and was neglected in this experiment.

The mini-slit was an annular passage, which was formed between the cylinder and an aluminum disk. This was also cut by CO_2 laser machine. Figure 3 is a photograph of alignment mechanism, in which climp-type terminals were set to align the cylinder with a disk utilizing screws of 2.6 mm. Table 2 is a list of disk diameter, which were 28.8, 28.5 and 28.0 mm. Corresponding slit width were 0.1, 0.25 and 0.5 mm.

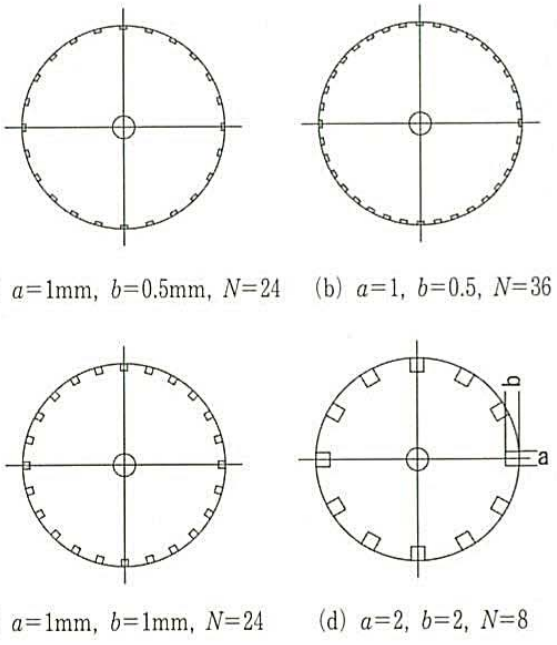

(a) a=1mm, b=0.5mm, N=24 (b) a=1, b=0.5, N=36

(c) a=1mm, b=1mm, N=24 (d) a=2, b=2, N=8

Figure 2 Plane views of mini-orifice elements.

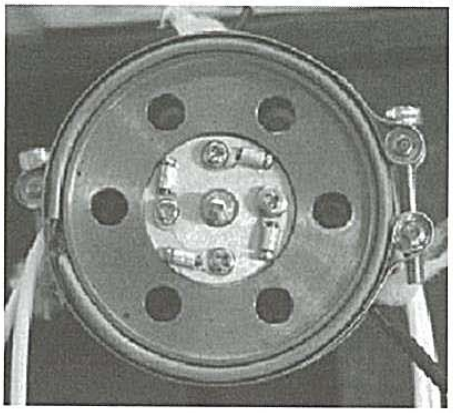

Figure 3 Photograph of mini-slit center alignment device viewed from bottom

Figure 4 (a) is a sectional view of minichannel array equipment with impingement flow system. Two minichannel array block were stacked with impingement distance of H=2.5 mm. In addition to impingement flow system, single stage minichannel array was also used. Figure 4 (b) is a plane view of minichannel array with 4 mm spacing between channels. These channels were identical to those used in reference (2). Dimensions of minichannel array is listed in Table 3.

Compressed air was supplied from a compressor of 2.2 kW to the equipment through an air dryer, a pressure regulator and mass flow meters. Mass flow meters of 200 litter/min were connected in parallel to allow the maximum flow rate of 400 litter/min. Temperature of the oxygen free copper block was controlled by thyristor temperature controller at 70℃. Three thermocouples were installed equally spaced around the cylinder, one of which is connected to the temperature controller. A mixing screen was set at upstream of exit thermocouple to measure mixed temperature. The temperature difference between upstream and downstream thermocouple was below 0.1℃ at the non-heating condition.

A back pressure valve was installed at the exit of the equipment for all test condition. The pressure at the downstream plenum was set 1 and 4 atmosphere for all tests. The pressure of 4 atmosphere was a feasible maximum pressure for compressor capability.

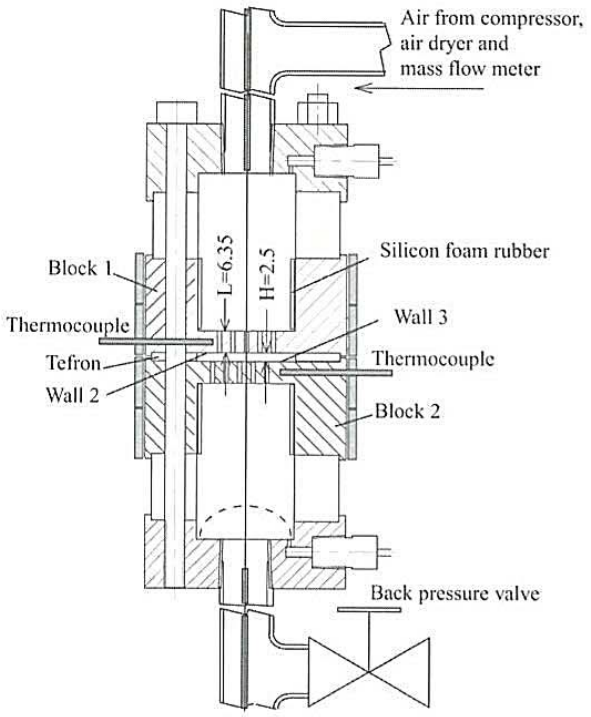

(a) Cross section

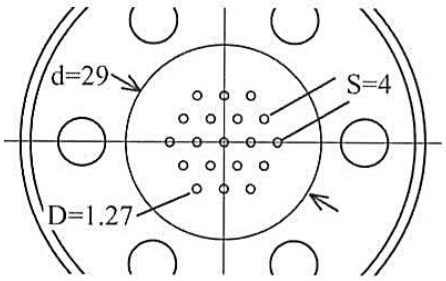

(b) plane view of the minichannel array

Figure 4 minichannel equipment with impingement jet flow

All dimensions of elements are expressed in mm, but unit of meter was used in the analysis.

Definition of Variables Reynolds number was defined by Equation (1) based on hydraulic diameter, viscosity and mass flow rate per an element or a channel.

$$R_e = \frac{mD_h}{\mu A} \tag{1}$$

Reynolds number is proportional to mass flow rate by the definition. Dimensionless temperature is defined by inlet temperature T_1, exit temperature T_2 and wall temperature T_w in Equation (2).

$$\theta = \frac{T_2 - T_1}{T_W - T_1} \tag{2}$$

Coefficient of power (*COP*) was defined as the ratio of convected thermal energy and pumping power to flow the coolant. We define *COP* only considering inlet and outlet of the elements, although various definitions can be possible for each practical application.

$$\frac{convection}{compression} = \frac{T_2 - T_1}{T_1}\left\{\left(\frac{P_1}{P_2}\right)^{\frac{\kappa-1}{\kappa}} - 1\right\}^{-1} \tag{3}$$

The pumping power was defined by the isentropic compression work of air from outlet pressure P_2 to inlet pressure P_1 for the inlet temperature T_1. The power did not include the additional pumping power of coolant to cool the temperature rise of isentropic compression to the inlet temperature T_1. In order to compensate room and wall temperature variation, Equation (3) was modified by multiplying $T_1/(T_w - T_1)$ to get *COP*.

$$COP = \theta\left\{\left(\frac{P_1}{P_2}\right)^{\frac{\kappa-1}{\kappa}} - 1\right\}^{-1} \tag{4}$$

Table 1 Mini-Orifice

	a	*b*	*N*	*D*h	*S*/*D*h
1	1	0.5	36	0.666	3.79
2	1	1	24	1	3.796
3	2	2	12	2	3.79
4	1	0.5	24	0.666	5.69
5	2	2	8	2	5.7

Table 2 Mini-Slit

	D	*c*	*D*h	*S*/*D*h
1	28.8	0.1	0.2	0
2	28.5	0.25	0.5	0
3	28	0.5	1	0

Table 3 Minichannel

	D	*L*	*N*	*H*	*D*h	*S*/*D*h
1	1.27	6.35	19	-	1.27	3.149
2	1.27	6.35	19	2.5	1.27	3.149

dimensions are in mm

RESULTS AND DISCUSSIONS

Result of minichannel array Figure 5 is dimensionless temperature θ plotted on Reynolds number for single and two stage minichannel array with downstream plenum pressure of 1 and 4 atmosphere conditions. Plots of group A are result for single stage minichannel. These show that θ decreased linearly with logarithm of Reynolds number and the heat transfer was not affected by system pressure variation. In other words, the temperature rise of heat exchanger was related to the mass flow rate. These characteristics of minichannel heat transfer were very similar to that of Dittus-Boelter correlation except low Reynolds number region. The Dittus-Boelter correlation is converted to Equation (5) by $S_t = N_u/(R_e P_r)$ relation.

$$S_t = 0.023 R_e^{-0.2} P_r^{-0.6} \tag{5}$$

The channel dimensionless temperature was estimated under constant wall temperature and con-

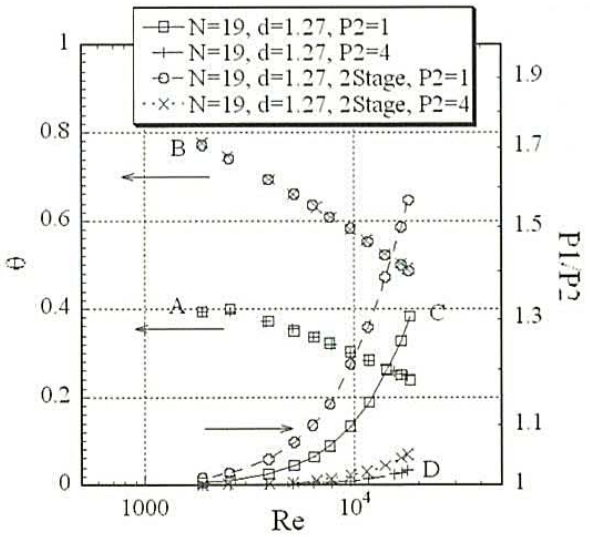

Figure 5 Dimensionless temperature and pressure ratio

stant heat transfer coefficient distribution along the axial direction in a channel to get Equation (6).

$$S_t = -\frac{D_h}{4L}\ln(1-\theta_C) \qquad (6)$$

Substituting Equation (5) into Equation (6), we can get relation of dimensionless temperature and Reynolds number, which was plotted with a parameter L/D_h in Figure 6. The dimensionless temperature also decreased linearly with logarithm of Reynolds number, although the magnitude was different from experiment. Experimental value of θ was about four times larger than calculated value for $L/D_h=5$. Reynolds or Chilton-Colburn analogy describes the relation between momentum and heat transfer in turbulent flow, if the solid surface is covered with viscous sub-layer. The analogy was completely realized in the minichannel, although the magnitude was different from each other. Figure 5 also shows that the dimensionless temperature was not affected by the system pressure variation. This is based on that thermal conductivity is not affected by pressure in this pressure level.

The pressure ratio P_1/P_2 was greatly affected by system pressure comparing the plot C for 1 atmosphere and plot D for 4 atmosphere in Figure 5. The pressure difference P_1-P_2 is replaced by $P_1-P_2=P_2\ (P_1/P_2-1)$, and P_1/P_2-1 can be seen in the right vertical axis of the figure because it started from 1. Finally, pressure difference of 4 atmosphere was smaller than that of 1 atmosphere, since P_1/P_2-1 was about one-tenth for high pressure operation. The pressure gradient, $\partial p/\partial r$, in the inlet region of the minichannel must be related to the pressure difference and decreased for high pressure operation. This may lead to a conclusion that the heat transfer was not affected by magnitude of the pressure gradient.

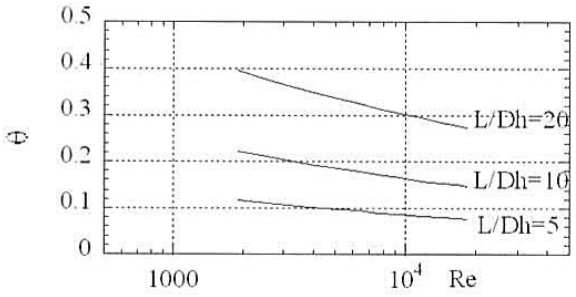

Figure 6 Calculated result of dimensionless temperature assuming Dittus-Boelter correlation

Result of mini-slit and mini-orifice In Figure 7 the dimensionless temperature is shown for the mini-slits. The result was similar to the result of minichannel in that the θ decreased linearly with logarithm of Reynolds number and did not depend on the system pressure variation. The θ increased for the narrow clearance of the slit. This is because the large part of air contacted to the heated wall when air passed through the clearance. The high pressure ratio was needed for high θ especially for $c=0.1$ mm slit.

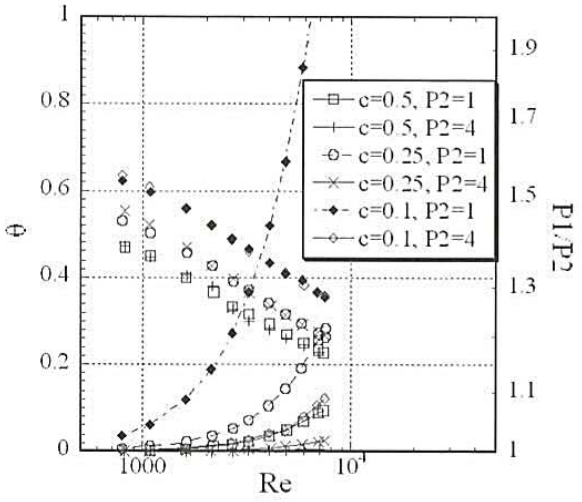

Figure 7 Dimensionless temperature and pressure ratio for mini-slit

The result of mini-orifice is shown in Figure 8 for system pressure of 1 atmosphere. The dimensionless temperature was similar to the result of minichannel and mini-slit. It decreased linearly with logarithm of Reynolds number both for 1 and 4 atmosphere, although the result for 4

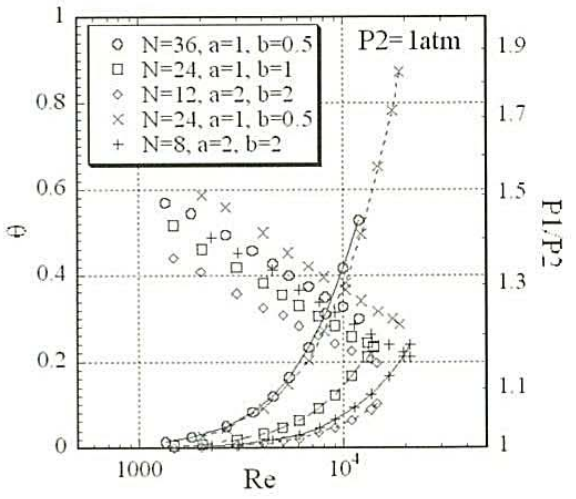

Figure 8 Dimensionless temperature and pressure ratio for mini-orifice

atmosphere is not shown here. Comparing the result of $a=1$, $b=0.5$ and $N=24$ to the result of $a=1$, $b=0.5$ and $N=36$, the θ was large for $N=24$. This means that θ was dependent on the spacing S of the elements.

Connection of mini-orifices in series Three mini-orifices were connected in series to get higher dimensionless temperature in two cases. In the first experiment, as assembled in Figure 9 (a), three disks of $a=1$, $b=0.5$, $N=24$ were used. First disk was located at $x=9.7$ mm from the cylinder edge, and 3 disks were stacked with 2.3 mm spacing. In the second experiment, the 3 disk unit was assembled in minichannel array block as shown in Figure 9 (b).

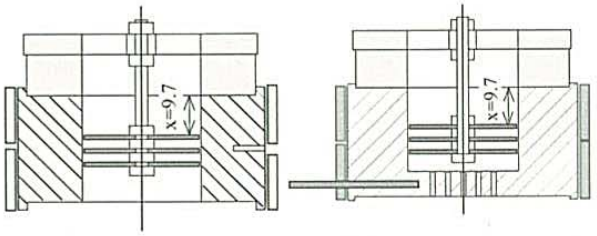

(a) mini-orifice (b) mini-orifice and minichannel

Figure 9 Stacked heat transfer test for mini-orifice of $N=24$, $a=1$, $b=0.5$ (left) and combined element with minichannel array (right)

Experimental result is shown in Figure 10 together with the case of stacking 1 and 2 disks assembly. The dimensionless temperature was not so much improved for 2 and 3 disks compared to the single disk mini-orifice. This may caused by decreasing cylinder inner surface for a disk.

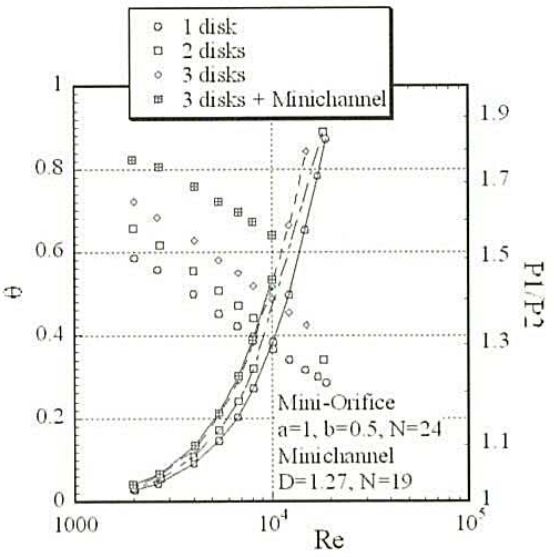

Figure 10 Dimensionless temperature and pressure ratio for elements shown in Figure 16

Coefficient of power The *COP* of the minichannel array is shown in Figure 11, where *COP* of 1 and 2 stage for system pressure of 1 and 4 atmosphere were plotted on Reynolds number. *COP*

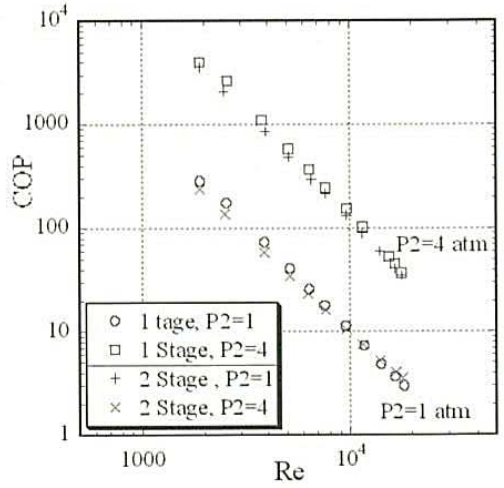

Figure 11 *COP* and Reynolds number for minichannel single stage and 2 stage impingement arrangement

was basically same for 1 and 2 stages, although the dimensionless temperature was obviously high for 2 stage minichannel array including impingement jet in Figure 5. This means that heat transfer indeed was improved by complicated structure of passage, but the energy consumption increased simultaneously and that resulting *COP* was not so changed. *COP* increased remarkably as the system pressure was increased to 4 atmosphere because the pressure loss was reduced by feeding high density and low velocity air in the minichannel for same flow rate. In summary, convected heat per unit mass kept unchanged while the energy to feed the unit mass of fluid changed.

COP of the mini-slit is plotted on Reynolds number in Figure 12. *COP* increased for large clearance of $c = 0.5$ mm and high system pressure of 4 atmosphere. For small clearance, more portion of supplied air was able to contact with heated surface than large clearance case providing high dimensionless temperature, but the energy of pressurizing air increased. *COP*-Reynolds number correlation for mini-orifice had similar characteristics with other configuration and will be discussed later.

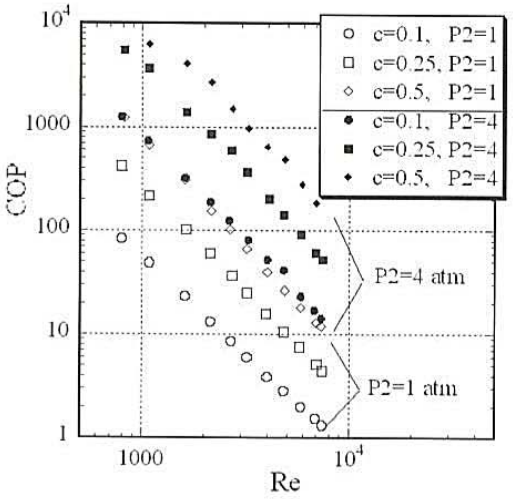

Figure 12 *COP* and Reynolds number for mini-slit elements in 1 and 4 atmosphere

Discussion on the impingement jet The plots of group B in Figure 5 shows dimensionless temperature of 2 stage impingement jet. The result was also not affected by system pressure variation. The mean value of momentum of the air in the minichannel is represented by Equation (7).

$$momentum = \rho u A \cdot u \tag{7}$$

, where u is channel mean velocity. The momentum of the impinging jet reduced to one fourth, because the term $\rho u A$ is identical for same flow rate due to the continuity equation and the mean velocity reduced to one fourth at the elevated pressure. The result of heat transfer, however, was hardly affected by momentum change between 1 and 4 atmosphere. This means that high jet velocity was not necessarily needed for impingement cooling and the pumping power may be saved if some optimization is done.

The magnitude of local pressure gradient at the wall 3 must be strong for reacting large momentum of the jet at low system pressure case (high jet velocity), in which dimensionless temperature was unchanged from high system pressure operation. This reveals that thermal convection did not depend on the magnitude of pressure gradient. This was also pointed out in the end of preceding paragraph for inlet of minichannel.

Unlike the dimensionless temperature, total convected heat of the system increased with increasing mass flow rate, although the figure was not shown in this paper. Local Nusselt number of the impinged surface in this experiment was considered to increase with increasing Reynolds number for given system pressure as was usually shown in many paper.

We now discuss about the relation between flow field and heat transfer by a certain quantity. As a first step we define a local Stanton number to normalize a local heat flux by Equation (8).

$$S_{tl} = \frac{W}{C_p (m/A)(T_w - T_1)} \tag{8}$$

In the second step, we introduce a parameter representing the qualitative character of the flow field. The deformation of flow field is represented by a velocity gradient tensor. Chong and Perry (1990) classified the velocity field by way of the eigen value of the velocity gradient tensor. But the classification was very complicated. We tried to introduce more simple parameter. The tensor is decomposed into two independent tensor of spin and rate of strain. We introduce the Truesdell kinematic vorticity number to characterize the flow field, which is the ratio of magnitude of spin and rate of strain tensor.

$$W_k=\sqrt{\left(\frac{\partial u_i}{\partial x_j}-\frac{\partial u_j}{\partial x_i}\right)\left(\frac{\partial u_i}{\partial x_j}-\frac{\partial u_j}{\partial x_i}\right)\Big/\left(\frac{\partial u_i}{\partial x_j}+\frac{\partial u_j}{\partial x_i}\right)\left(\frac{\partial u_i}{\partial x_j}+\frac{\partial u_j}{\partial x_i}\right)} \tag{9}$$

The value is unity for simple shear layer and is infinity for flow field of solid vortex because the rate of strain is zero. In the flow field of streamwise vortex, the kinematic vorticity number has a value of greater than unity, and the eigen value of velocity gradient tensor is imaginary number which represents a vortical flow around some axis of rotation. The value is less than unity in the stagnation or accelerated flow field, if the flow does not entrain a vorticity. The kinematic vorticity number corresponds to various kinds of flow fields. Deformation field is linked with static pressure field by Equation (10), which was given in Kida and Yanase (1999) and was modified by the author to include W_k explicitly.

$$\frac{4}{\rho}\nabla^2 P=\left(W_k^2-1\right)\left(\frac{\partial u_i}{\partial x_j}+\frac{\partial u_j}{\partial x_i}\right)\left(\frac{\partial u_i}{\partial x_j}+\frac{\partial u_j}{\partial x_i}\right) \tag{10}$$

It is difficult to interpret the behavior of this equation in the flow field because of Laplacian. But for simple shear layer, W_k is unity and the Laplacian of the static pressure is zero, then pressure gradient is constant and the example of the flow field is Hagen-Poiseuille or Couette flow. If the value of W_k is less than unity, boundary layer is influenced by favorable or adverse pressure gradient more than simple shear layer in the way that boundary layer was stretched or squeezed in the flow direction in the flow field very close to the wall. Concerning the heat transfer, the parameter of interest is a velocity gradient at the wall, which is affected by the pressure field where W_k is less than unity. The state of deformation of boundary layer can be roughly expressed by the value of the kinematic vorticity number.

Both the spin and rate of strain tensor can be easily obtained from CFD solver. The result of Hara et al[2] was appropriate to show the Stanton number and the kinematic vorticity number. The W_k was defined at the grid point most close to the wall, where the value of $y+$ was greater than 10. The velocity field at the second grid point, however, was affected by the pressure gradient. The W_k was not always unity even if the wall function was applied.

Figure 13 shows distributions of Stanton number and kinematic vorticity number on wall 3, which is defined in Figure 4. The Stanton number distribution was a same figure that has already been reported in reference (2). A black circles 'A' represents minichannels of 1.27 mm diameter machined in block 2. A white circles 'B' are projection of minichannels in block 1 and the jets impinge against wall 3. Pseudo limiting streamlines were drawn by means of velocity fields most close to the wall and superimposed on the figure. Stream lines gathered around 'D', the centroid of impingement points, and flowed back to wall 2 as a 'fountain'.

The Stanton number was high at the impingement region 'B' as expected. The kinematic vorticity number was less than unity because the fluid deformation was larger than simple shear layer. The large value of local Stanton number in this region was caused by the un-heated air approaching the stagnation region (temperature difference) and may be caused by large velocity gradient normal to the wall (temperature

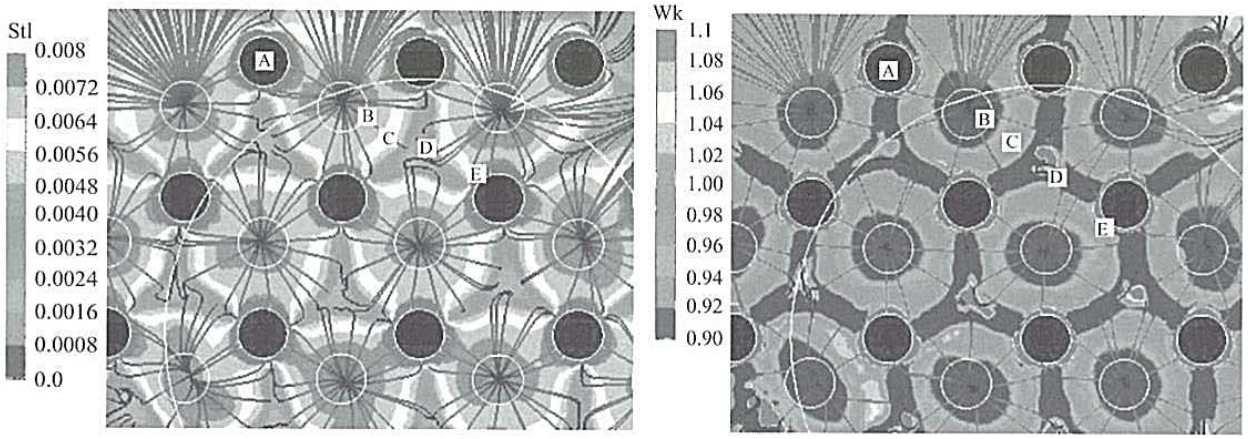

(a) Stanton number on wall 3

(b) Kinematic vorticity number on wall 3

Figure 13 Stanton number and kinematic vorticity number on wall 3 at pressure ratio=1.8

gradient). The kinematic vorticity number, however, closed to unity near 'C' as the streamlines extended apart from the stagnation region. The pressure gradient changed from favorable to adverse along the streamline during 'B' to 'D'. The Stanton number was low around 'D'. This was caused by already heated air in the stagnation region 'B' and small velocity gradient normal to the wall.

The point 'D' was also a stagnation region, where kinematic vorticity number decreasedl once again along the streamline beyond 'C'. The number, however, exceeded unity at the center where they were colored by red. The reason was that the flow entrained vorticity to the stagnation point. Contrary to point 'B', the flow direction was alternate to the stagnation point near 'D'. The streamline revealed that flow field had vortical structure normal to the wall. These structure, however, did not contribute to the heat transfer.

The kinematic vorticity number was larger than unity around the channel inlet 'E'. This suggested the ring-like vortical structure. Due to the authors knowledge, however, such a vortical flow was not observed at very high favorable pressure gradient region. A CFD analysis of very high spatial resolution might be needed to clarify the flow field around the channel inlet.

The kinematic vorticity number was one of the scalar quantity, which can connect the flow field and heat transfer although the advantage reduced because the value corresponded to both large and small Stanton number region.

The heat transfer including impingement jet also belonged to the category of the Reynolds analogy, because the dimensionless temperature also decreased linearly with logarithm of Reynolds number for 1 and 4 atmosphere in Figure 5. It is usually said that the impingement heat transfer was correlated to the turbulence intensity in the wall jet region. The author, however, has no comments on this issue, because there is no evidence about the relation between turbulence and surrounding pressure in this experiment.

The fact that θ did not depend on the momentum of the impinging jet, reveals that the name 'stagnation heat transfer' is more appropriate than 'impingement heat transfer' to the thermal convection in this region. The impingement heat transfer may be considered as a phenomena that some part of air in the jet 'newly' contacts with the heated surface and heat convected effectively.

Separation of heat transfer around the minichannel inlet For mini-orifice and mini-slit, it is very difficult to separate convected heat inside the channel from total heat convected, because the thickness of the aluminum disk is only 1 mm. In order to discuss about factors affecting heat transfer in the minisized heat transfer elements of 3 types, convected heat in the mini-channel should be subtracted from total heat convection. As a matter of fact, experimental separation of this is very difficult. Inlet heat transfer can be estimated by the following method. Air was heated to dimensionless temperature θ_I on the inlet plane, then heated by a part of dimensionless temperature θ_C in the minichannel according to Dittus-Boelter correlation. Air was finally heated to θ at the exit of the channel and flowed out to the downstream plenum. Assuming constant wall temperature, the overall dimensionless temperature θ is represented by Equation (11).

$$\theta=\theta_I+(1-\theta_I)\theta_C \tag{11}$$

θ_I can be defined by θ_C from Equation (6) and θ from experimental data. Figure 14 (a) is a comparison between these dimensionless temperatures showing that heat transfer was active on the inlet plane of the channel. Then we can define Equation (12) by the ratio of θ_I and θ_C as a minichannel gain.

$$G_5=\frac{\theta_I}{\theta_C} \tag{12}$$

The subscript '5' is used because the value is based on $L/D_h=5$. Figure 14 (b) is a distribution of G_5 for 1 and 4 atmosphere gradually decreasing for high Reynolds number region. This means that heat transfer on the inlet plane decreased more than channel itself but did not depend on the pressure. Overall dimensionless temperature can be estimated for given Reynolds number by calculating θ_I from Equation (6) using the θ_C for $L/D_h=5$ and θ_C for given L/D_h.

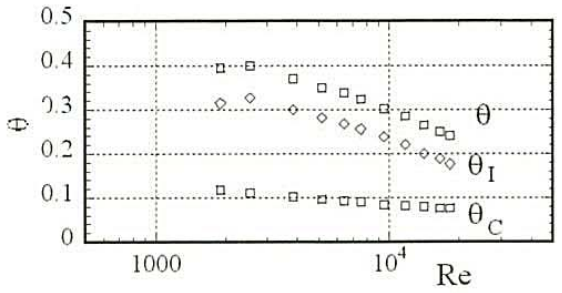

Figure 14 (a) Estimated dimensionless temperature for channel inlet

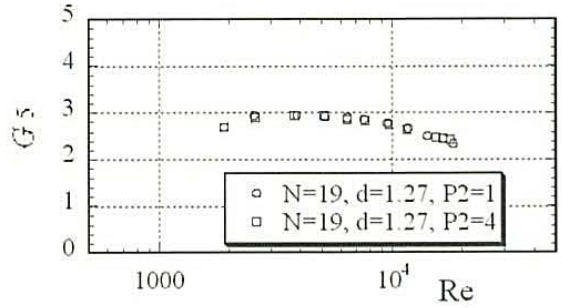

Figure 14 (b) Minichannel gain defined by Equation (6)

Factors affecting the heat transfer An overall dependency of heat transfer on shapes and dimensions of the elements were investigated by extracting θ from experimental θ - R_e relation, (Figure 5, 7 and 8) utilizing numerical regression method for constant Reynolds number and constant pressure ratio respectively.

Figure 15 is a plot of dimensionless temperature on the hydraulic diameter of the elements at Reynolds number=10,000. The parameter S/D_h is a dimensionless distance between neighboring elements and is zero for mini-slit since number of element is one. Figure 15 showed that θ increased for small hydraulic diameter elements. θ also increased with S/D_h. This dependency was caused by the increasing convection area per an element for large S/D_h. For minichannel array, however, θ_I was plotted to compare the convection of channel inlet region. The value of θ_I matched with dimensionless temperature of other elements although the shape of the heat transfer element was very different.

Figure 16 is similar to Figure 15, which also

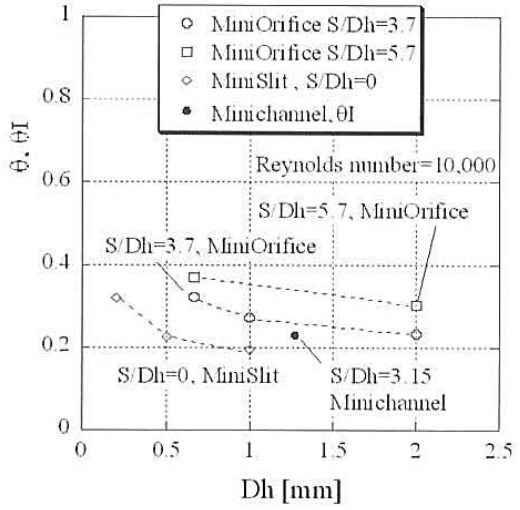

Figure 15 Correlation of dimensionless temperature and hydraulic diameter for Reynolds number=10,000

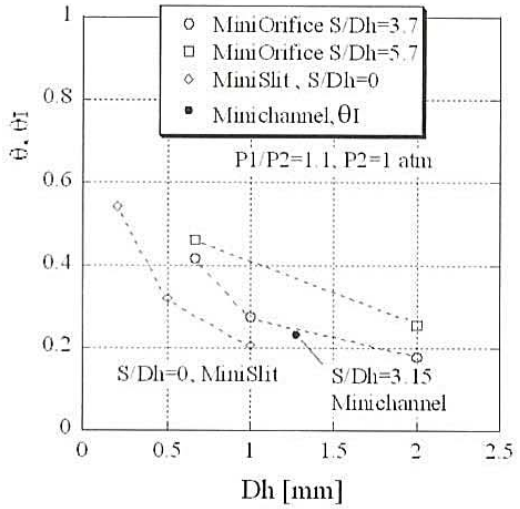

Figure 16 Correlation of dimensionless temperature and hydraulic diameter for pressure ratio=1.1

plots dimensionless temperature on the hydraulic diameter for constant pressure ratio of P_1/P_2 =1.1. This may be more possible operation for general working condition of small elements as a heat exchanger system. In this case, the mass flux m/A is almost constant, and Reynolds number is small for small D_h element from Equation (1). θ increased more for small hydraulic diameter than the case of constant Reynolds number condition of Figure 15, since Reynolds number was low for small D_h element and θ was large for low Reynolds number. Author guessed that D_h/A was the dominant parameter of heat transfer because of large ratio of wetted perimeter length to cross-sectional area of the channel. This is based on that the heat transfer is concerned with wetted perimeter length and the mass flow rate is concerned with cross-sectional area. This was true for mini-orifice, but was not true for mini-slit. It may be concluded in any case that the convection of small element depended on its size from these two figures. More experiment of minichannel is needed to conclude the problem.

Figure 17 is a correlation of *COP* and D_h at Reynolds number=5,000 and 10,000 for P_2 =1 atm. The *COP* increased almost linearly with D_h and was very little for small D_h elements. This was caused by the high pressure ratio required to realize specified Reynolds number for small element.

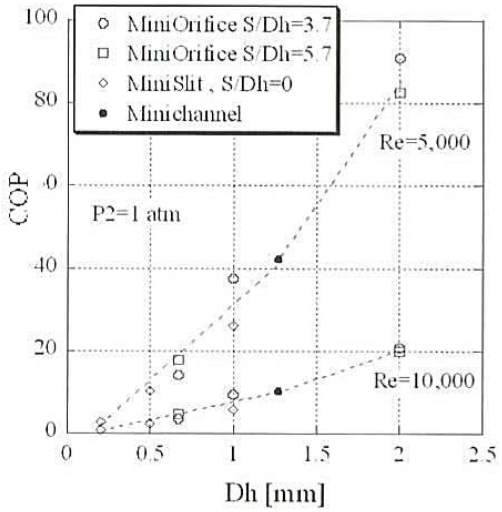

Figure 17 Correlation of *COP* and hydraulic diameter for Reynolds number=5,000 and 10,000 for P_2=1 atm

Figure 18 is a correlation of *COP* and D_h at pressure ratio=1.1 and P_2=1 atm. The patterns of the *COP* were same to θ in Figure 16, since the pressure ratio was constant in Equation (4). Because the total convected heat was used to

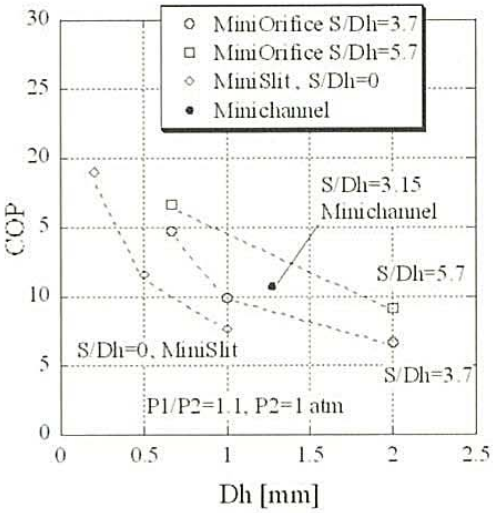

Figure 18 Correlation of *COP* and hydraulic diameter for pressure ratio=1.1 and P_2=1 atm

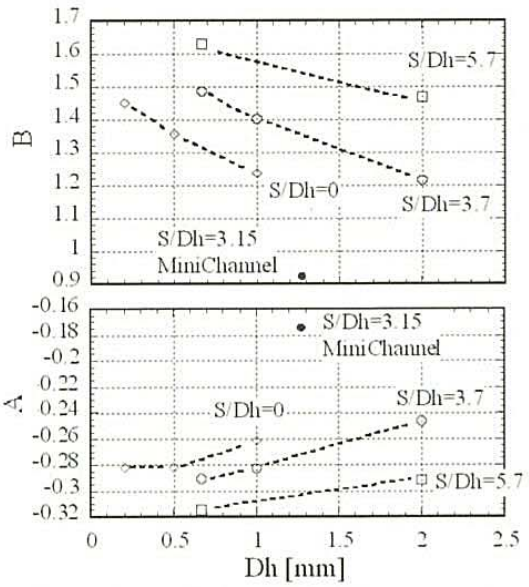

Figure 19 coefficients of linear regression defined in Equation (13)

evaluate *COP*, the plot for minichannel was different in Figure 18.

The dimensionless temperature was considered to be a function of hydraulic diameter D_h, dimensionless distance S/D_h and Reynolds number. Then, relation between θ and Reynolds number for each element was assumed to have a form of Equation (13) using regression analysis.

$$\theta = A\log_{10} R_e + B \qquad (13)$$

The coefficient A and B were plotted on hydraulic diameter to get Figure 19. Coefficient A and B can be interpolated for given D_h and S/D_h to get θ for mini-orifice element. The similar relation can be obtained for minichannel, if experiment is done for several sets of diameter and S/D_h.

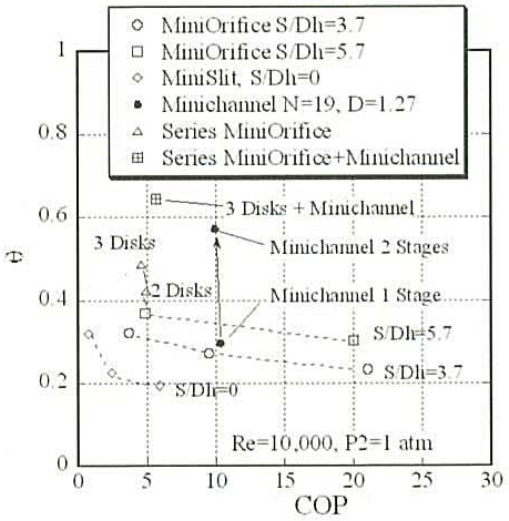

Figure 20 Correlation of dimensionless temperature and *COP* for Re=10,000 and P_2=1 atm.

A qualitative guide for cooling design Figure 20 is a correlation of θ and *COP* at R_e=10,000 and P_2=1 atm to understand the overall character of the heat exchanger including series connection of the elements. The same correlation for constant pressure ratio may lose its meaning be cause θ is exactly proportional to *COP*. For single elements, dimensionless temperature increased as the *COP* decreased and vice versa. As we have already observed in Figure 12 for the series connection of minichannel array that *COP* was affected little by the series connection of elements, we can observe more clearly this comparing the minichannel of 1 stage and 2 stage plot. The increase of θ was necessarily accompanied by decrement of *COP*, which was larger for series connection of a=1, b=0.5, N=24 mini-orifice than series connection of minichannel array. The decrement of *COP* for series connection, however,

was smaller than the case of improving θ by means of smaller sized single element.

From the fact that we have investigated, some guidelines has revealed that series connection of moderate *COP* elements was effective to get high θ and high *COP* simultaneously. The target value of dimensionless temperature is about 0.8 in the modern gas turbine blade cooling (Wilcock et al, 2005) . Realization of this value, however, needs many stacks unless Reynolds number is low. The element of small size has disadvantage to design an efficient cooling system. The size of element should be as large as possible, if the elements can be packed into a certain space.

CONCLUSIONS

Heat transfer characteristics was investigated for three kinds of heat transfer elements; minichannel array, minisized orifice and minisized slit.

1. The dimensionless temperature decreased linearly with logarithm of Reynolds number for all configuration and system pressure of 1 and 4 atmosphere. This means that heat transfer was strongly controlled by Reynolds or Chilton-Colburn analogy and was determined by thermal conduction in the viscous layer on the metal surface.

2. The convected heat in the inlet plane of the minichannel was estimated by subtracting channel heat transfer estimated by Dittus-Boelter correlation from measured heat transfer, because the result of minichannel array heat transfer had similar functional nature to the integrated result of Dittus-Boelter correlation. The dimensionless temperature of the channel inlet plane achieved about three times greater than that of channel heat transfer.

3. The dimensionless temperature was a function of Reynolds number, hydraulic diameter D_h and the ratio of distance between elements S/D_h. It increased as D_h became small and S/D_h became large. This means that the area of heat transfer increased as S/D_h became large.

4. The dimensionless temperature of a certain configuration can be estimated by using above three factors for mini-orifice.

5. The dimensionless temperature was not affected by system pressure variation for all experiment. This was also true for impingement jet system. This means that the momentum of the jet did not affect the impingement heat transfer.

6. *COP* increased linearly with the size of element. Use of small size element deteriorates efficient cooling design although it can achieve high dimensionless temperature.

7. In the series connection of heat transfer elements, dimensionless temperature increased with little decrease of *COP*.

REFERENCES

[1] Hara, K., Furukawa, M., and Akihiro, N., 2005, ' Experimental Investigation of Heat Transfer in Square And Circular Minichannel Air Flow for Wide Range of Pressure Ratio ', ICMM2005-75184

[2] Hara, K., Furukawa, M., and Akihiro, N., 2006, 'Experimental and Numerical Analysis of High Heat Transfer Phenomenon in Mini-channel Gaseous Cooling', ICNMM2006-96213, This paper will be published from Journal of Turbomachinery, Transactions of the ASME

[3] Chong, M. S. and Perry, A. E., 1990,`A General Classification of Three-Dimensional Flow Fields', Phys. Fluids A 2 (5), p. 765

[4] Kida, S., Yanase, S., 1999, 'Turbulent Dyn amics', Asakura Shoten Tokyo (in Japanese)

[5] Wilcock, R. C., Young, J. B., Horlock, J. H., 2005, 'The Effect of Turbine Blade Cooling on the Cycle Efficiency of Gas Turbine Power Cycles', Journal of Engineering for Gas Turbines and Power Transactions of the ASME, vol. 127, p. 109-120